

# Linear and non-linear bias: predictions vs. measurements

K. Hoffmann<sup>1</sup>, J. Bel<sup>2</sup>, E. Gaztañaga<sup>1</sup>

<sup>1</sup>*Institut de Ciències de l’Espai (ICE, IEEC/CSIC), E-08193 Bellaterra (Barcelona), Spain*

<sup>2</sup>*Aix Marseille Univ, Univ Toulon, CNRS, CPT, Marseille, France*

Received date / Accepted date

## ABSTRACT

We study the linear and non-linear bias parameters which determine the mapping between the distributions of galaxies and the full matter density fields, comparing different measurements and predictions. Associating galaxies with dark matter haloes in the MICE Grand Challenge N-body simulation we directly measure the bias parameters by comparing the smoothed density fluctuations of haloes and matter in the same region at different positions as a function of smoothing scale. Alternatively we measure the bias parameters by matching the probability distributions of halo and matter density fluctuations, which can be applied to observations. These direct bias measurements are compared to corresponding measurements from two-point and different third-order correlations, as well as predictions from the peak-background model, which we presented in previous articles using the same data. We find an overall variation of the linear bias measurements and predictions of  $\sim 5\%$  with respect to results from two-point correlations for different halo samples with masses between  $\sim 10^{12} - 10^{15} h^{-1} M_{\odot}$  at the redshifts  $z = 0.0$  and  $0.5$ . Variations between the second- and third-order bias parameters from the different methods show larger variations, but with consistent trends in mass and redshift. The various bias measurements reveal a tight relation between the linear and the quadratic bias parameters, which is consistent with results from the literature based on simulations with different cosmologies. Such a universal relation might improve constraints on cosmological models, derived from second-order clustering statistics at small scales or higher-order clustering statistics.

**Key words:** methods: analytical - methods: statistical - galaxies: haloes - dark matter - large-scale structure of Universe.

## 1 INTRODUCTION

The increase of data from upcoming and next generation of galaxy surveys is pulling down errors on the observed statistics of the large-scale galaxy distribution. Thus, the inferences on cosmological models from these statistics requires a modeling of cosmological fluids and their statistical properties with an accuracy of at least the same order of magnitude as the observational errors.

One of the largest uncertainties comes from the modeling of the mapping between the observed fluctuations of galaxies to the fluctuation of the underlying matter distribution (hereafter referred to as  $\delta_g$  and  $\delta_m$  respectively). These fluctuations are defined as normalized deviations of the density  $\rho$ , smoothed typically with a top-hat window of characteristic scale  $R$ , from the mean density of the universe  $\bar{\rho}$  at the position  $\mathbf{r}$ ,

$$\delta(\mathbf{r}) \equiv \frac{\rho(\mathbf{r}) - \bar{\rho}}{\bar{\rho}}. \quad (1)$$

The mapping from  $\delta_g$  to  $\delta_m$  is described by the so-called bias function,  $\delta_g = F[\delta_m, \nabla_{ij}\Phi_v]$ , where  $\nabla_{ij}\Phi_v$  are second order derivatives of the velocity potential. The latter relate  $\delta_g$  to the matter distribution beyond the smoothing scale  $R$  and are therefore referred as *non-local* contributions to the bias model (Chan et al. 2012; Baldauf et al. 2012). For sufficiently large smoothing scales such non-local contributions may be negligible, which allows for a local description of biasing. Thus, the bias function can be modeled as a Taylor expansion in terms of the matter fluctuations (Fry and Gaztanaga 1993)

$$\delta_h = F[\delta_m] \simeq \sum_{i=0}^N \frac{b_i}{i!} \delta_m^i, \quad (2)$$

where  $b_i$  are the bias parameters. However, for smaller smoothing scales, which are typically used for studying the two- and three-point statistics of the galaxy distribution, non-local contributions need to be considered. When fluctuations in the density and velocity potential of the matter distribution are sufficiently small the non-local bias model

may be described by its second-order expansion, which is hereafter referred to as non-local quadratic bias model

$$\delta_g = b_1 \left\{ \delta_m + \frac{1}{2} [c_2 (\delta_m^2 - \langle \delta_m^2 \rangle) + g_2 \mathcal{G}_2] \right\}, \quad (3)$$

where  $b_1$  and  $c_2 \equiv b_2/b_1$  are referred to as linear and quadratic (or second-order) bias parameters respectively. The non-local contribution to the bias function consists in that case of the product of the second-order non-local bias parameter  $g_2$  and the smoothed second-order Gallileon

$$\mathcal{G}_2(\mathbf{r}) = \int \beta_{12} \theta_v(\mathbf{k}_1) \theta_v(\mathbf{k}_2) \hat{W}[k_{12}R] e^{i\mathbf{k}_{12} \cdot \mathbf{r}} d^3\mathbf{k}_1 d^3\mathbf{k}_2, \quad (4)$$

where  $\mathbf{k}_i$  and  $\mathbf{k}_{12} \equiv \mathbf{k}_2 - \mathbf{k}_1$  are wave vectors of density oscillations,  $\beta_{12} \equiv 1 - (\hat{\mathbf{k}}_1 \cdot \hat{\mathbf{k}}_2)^2$  represents the mode-coupling between density oscillations which describes tidal forces,  $\theta_v \equiv \nabla^2 \Phi_v$  is the divergence of the normalized velocity field ( $\mathbf{v}/\mathcal{H}/f$ ) and  $\hat{W}[k_{12}R]$  is the window function in Fourier space. Note that in the case  $g_2 = 0$  equation (3) corresponds to the local quadratic bias model.

The bias parameters are highly relevant for constraining cosmological models via the growth of matter fluctuations, derived from second-order statistics of the observed galaxy distribution. In particular at large scales, the linear bias factor  $b_1$  is completely degenerate with the linear growth factor. Hence, growth-independent measurements of  $b_1$  can strongly tighten cosmological constraints from galaxy surveys.

Third-order statistics probes the linear and quadratic bias parameters independently of the growth and can be used to break the growth-bias degeneracy in the second-order statistics. Furthermore, the second-order bias measurements from third-order statistics allow growth measurements from second-order statistics at small scales, where non-linear and non-local terms contribute significantly to the signal. Such a small scale analysis would strongly improve the cosmological constraining power of galaxy surveys.

However, the value of combining second- with third-order statistics for constraining cosmological models with high precision arises from a detailed understanding of how exactly the bias parameters enter these statistics at different scales, redshifts and for different samples of tracers.

We therefore investigated in previous works (Hoffmann et al. 2015b; Bel et al. 2015, where the latter is hereafter referred to as paper I) how accurately the linear bias can be measured from different third-order statistics. These studies were based on the large cosmological MICE Grand Challenge (hereafter referred to as MICE-GC) N-body simulation in which haloes were detected as tracers of the cosmic web and associated with galaxies. The fact that the dark matter distribution is accessible in simulations allows for reliable measurements of the linear bias via second-order statistics, which can then be used as a reference for validating linear bias measurements from third-order statistics as well as theory predictions. Note that a reliable reference for validating higher order bias is currently only provided by running *separate universe* N-body simulations (Wagner et al. 2015; Lazeyras et al. 2015), which is beyond the scope of this article.

Alternatively to growth-independent bias measure-

**Table 1.** Abbreviations for previous articles of this series.

name in the text	reference
paper I	Bel et al. (2015)
paper II	Hoffmann et al. (2015a)

ments from third-order statistics one can employ bias predictions from the peak-background split model for breaking the growth-bias degeneracy. In Hoffmann et al. (2015a, hereafter referred to as paper II) we tested linear bias predictions in the MICE-GC simulations, confirming reports on inaccuracies of these predictions in the literature on a larger mass range thanks to the large volume and resolution of the MICE-GC simulation. As in case of the third-order statistics no reliable measurements for validating the predicted non-linear bias parameters were available. However, an interesting outcome of this analysis was a simple universal relation between the linear and non-linear bias parameters in the peak-background split model, which is independent of redshift and cosmology for halo samples with  $b_1 \gtrsim 2$ .

In the present work we conclude our series of articles, presenting results from an other method for allowing to measure bias parameters in the MICE-GC simulation. This method is based on a direct comparison of the halo and matter density fluctuations and may therefore be seen as the most direct way of measuring bias parameters. We also study a variant of this method, which is based on abundance matching of tracers and matter density contrasts. The interest of this alternative method is that it can be applied in galaxy surveys to estimate to bias function. Both methods deliver linear, as well as non-linear bias measurements. We compare these new measurements with the most reliable results from our previous work (paper I and II, see Table 1), which allows for the validation of how well bias can be measured with each approach. The different measurements of linear and non-linear bias parameters furthermore allow for a validation of the universal relation between the bias parameters, which we found for peak-background split predictions in paper II.

The remainder of this article is organised as follows. In Section 2 we describe the MICE-GC simulation as well as the halo samples on which our analysis is based on. The different methods for obtaining the bias parameters are briefly reviewed in Section 3, while details on bias measurements from the comparison of density contrasts are given in the appendix. We present our results in Section 4 which we summarize and discuss in Section 5.

## 2 SIMULATION AND HALO SAMPLES

Our analysis is based on the Grand Challenge run of the Marenstrum Institut de Ciències de l'Espai (MICE) simulation suite to which we refer to as MICE-GC in the following. Starting from small initial density fluctuations at redshift  $z = 100$  the formation of large scale cosmic structure was computed with  $4096^3$  gravitationally interacting collisionless dark matter particles in a  $3072 h^{-1} \text{Mpc}$  box using the GADGET - 2 code (Springel 2005) with a softening length of  $50 h^{-1} \text{kpc}$ . The initial conditions were generated using the Zel'dovich approximation and a CAMB power spectrum with the power law index of  $n_s = 0.95$ , which was normalised

**Table 2.** Halo mass samples used in this study.  $N_p$  is the number of dark matter particles per halo,  $N_{halo}$  is the number of haloes per sample in the comoving output at redshift  $z = 0.5$ .

sample	mass range [ $10^{12}h^{-1}M_{\odot}$ ]	$N_p$	$N_{halo}$
M0	0.58 - 2.32	20-80	122300728
M1	2.32 - 9.26	80-316	31765907
M2	9.26 - 100	316-3416	8505326
M3	$\geq 100$	$\geq 3416$	280837

to be  $\sigma_8 = 0.8$  at  $z = 0$ . The cosmic expansion is described by the  $\Lambda$ CDM model for a flat universe with a mass density of  $\Omega_m = \Omega_{dm} + \Omega_b = 0.25$ . The density of the baryonic mass is set to  $\Omega_b = 0.044$  and  $\Omega_{dm}$  is the dark matter density. The dimensionless Hubble parameter is set to  $h = 0.7$ . More details and validation test on this simulation can be found in Fosalba et al. (2013).

Dark matter haloes were identified as Friends-of-Friends groups (Davis et al. 1985) with a linking length of 0.2 in units of the mean particle separation. These halo catalogs and the corresponding validation checks are presented in Crocce et al. (2013). In the present analysis we use the dark matter field as well as haloes in the comoving outputs at redshift  $z = 0.0$  and  $0.5$ . The haloes are thereby divided into the four redshift independent mass samples M0 - M3 (defined in Table 2), which span a mass range from Milky Way like haloes up to haloes of massive galaxy clusters.

### 3 BIAS ESTIMATORS

In this section we summarize the different methods for measuring and predicting linear and non-linear bias parameters. An overview over the methods with the abbreviations and references for the corresponding bias is given in Table 3.

#### 3.1 $\delta_h - \delta_m$ relation

In simulations we can measure the density contrasts of haloes and matter (hereafter referred to as  $\delta_h$  and  $\delta_m$  respectively), which allows us to directly estimate the bias parameters  $b_i$  in equation (2). Here we briefly describe the two methods which we employ for these measurements, while more details are provided in the appendix of this article.

The first method has been widely used in the literature and may be seen as the most direct way to measure bias, provided that the biasing function is deterministic and local. It consists in fitting a polynomial to the  $\delta_h(\mathbf{r}_i) - \delta_m(\mathbf{r}_i)$  relations, which can be measured from the smoothed density fields of haloes and matter at different positions  $\mathbf{r}_i$  in the simulation. The best fit parameters are then identified as the bias parameters. Note that the parameter  $b_0$  is in principle constrained by requiring that by definition the average of the halo density contrast is null,  $\langle \delta_h \rangle = 0$ . We will refer to this method as  $\delta_h - \delta_m$  method in the remainder of this article. In practice, for obtaining the bias parameters  $b_1$ ,  $c_2 \equiv b_2/b_1$  and  $c_3 \equiv b_3/b_1$  we truncate the polynomial at third order. One can expect that this truncation introduces a dependence of the bias parameters on the smoothing scale, used to measure the density contrasts. At large smoothing scales the

matter fluctuations  $\delta_m$  are sufficiently small, hence a truncation of the bias function at  $\delta_m^3$  is adequate, whereas at small smoothing scales the stronger fluctuations would actually require an expansion beyond third order. Note that it is not clear that the Taylor expansion of the bias function beyond third order converges at smaller smoothing scales. Furthermore we expect the local deterministic bias to describe the mapping between matter and haloes only on sufficiently large smoothing scales. In fact we find a strong scale dependence of our bias measurements at small smoothing radii  $R$ , while results converge for scales larger than  $R = 40 h^{-1}\text{Mpc}$  (see Appendix or Manera and Gaztañaga 2011). We therefore only use scales between  $40 < R < 80 h^{-1}\text{Mpc}$  to derive the bias parameters via the  $\delta_h - \delta_m$  method.

The second method for measuring bias parameters from the  $\delta_h - \delta_m$  relation consists in matching the probability distributions (PDFs) of  $\delta_h$  and  $\delta_m$  and will therefore be referred to as the  $\delta$ PDF method in the following. As the  $\delta_h - \delta_m$  method it relies on the assumption that the bias function is local and deterministic which might distort the measurements, in particular at small smoothing scales as discussed above. However, the  $\delta$ PDF method has the advantage that it can be applied to observations since the PDF of matter fluctuations can be modelled for a given cosmology and the PDF of galaxies can be directly observed from redshift surveys (see Bel et al. 2016; Di Porto et al. 2014; Marinoni et al. 2005; Bernardeau et al. 2002). Inferring the bias from the  $\delta_h - \delta_m$  method, on the other hand, requires adequate observations for measurements of  $\delta_m$  via weak gravitational lensing and introduces additional uncertainties (Chang et al. 2016; Pujol et al. 2016). More details on the  $\delta$ PDF method can be found in the Appendix.

#### 3.2 two-point cross-correlation

The bias function in equation (3) has an important application in the cosmological analysis of galaxy clustering statistics, since it provides a parametrization of the deviation between the clustering of haloes (or galaxies) and the underlying matter distribution. In simulations, where the clustering of matter can be directly measured, one can infer the bias parameters by comparing the clustering statistics of haloes and matter. In this subsection we focus on bias measurements from the two-point correlation  $\xi$  as statistical measure for the clustering. It directly probes the linear growth factor, thereby providing strong constraints on cosmological models. The two-point correlation can be defined in configuration space as the mean product of density fluctuations  $\delta_i$  at the positions  $\mathbf{r}_1$  and  $\mathbf{r}_2$  that are separated by the distance  $r_{12} \equiv |\mathbf{r}_1 - \mathbf{r}_2|$ ,

$$\xi_{xy}(r_{12}) \equiv \langle \delta_x(\mathbf{r}_1)\delta_y(\mathbf{r}_2) \rangle = \langle \delta_x^1 \delta_y^2 \rangle(r_{12}). \quad (5)$$

The indices  $x$  and  $y$  refer to the density fields of haloes (or galaxies) and matter, while  $\langle \dots \rangle$  denotes the average over pairs of any orientation and position. The two-point auto-correlation (hereafter referred to as 2pc) corresponds to the case  $x = y$  and will be denoted in the following as  $\xi_h \equiv \xi_{hh}$  and  $\xi_m \equiv \xi_{mm}$  for halos and matter respectively, whereas the halo-matter cross-correlation (hereafter referred to as 2pcc) will be denoted as  $\xi^{\times} \equiv \xi_{hm}$ . Inserting the local bias model from equation (3) into equation (5) provides, at leading order, a simple relation between  $\xi_m$  and  $\xi^{\times}$ ,

$$\xi^\times(r_{12}) \simeq b_1 \xi_m(r_{12}) + \mathcal{O}[\xi_m^2]. \quad (6)$$

At large scales ( $r_{12} \gtrsim 20h^{-1}\text{Mpc}$ ), where the two-point correlation function is small, we expect  $\mathcal{O}[\xi_m^2]$  to be negligible (see e.g. paper I), which allows for measurements of the linear bias as

$$b_\xi^\times(r_{12}) \equiv \sqrt{\frac{\xi^\times(r_{12})}{\xi_m(r_{12})}} \simeq b_1. \quad (7)$$

We showed in paper I that  $b_\xi^\times$  is a reliable estimate of the linear bias  $b_1$ , since it agrees with various other estimators from second-order one- and two-point statistics at large scales.

### 3.3 three-point auto- and cross-correlations

Third-order statistics is sensitive to the shapes of large-scale density fluctuations. It therefore provides information about the large-scale structure which is not accessible with second-order one or two-point statistics as the latter is defined isotropically in configuration space. Combining second- and third-order statistics therefore allows for breaking the degeneracy between the linear growth factor and the linear bias parameter which otherwise limits the accuracy of cosmological constraints derived from the 2pc at large scales (see e.g. Bernardeau et al. 2002, or paper I). However, this approach relies on the accuracy with which the linear bias can be measured with third-order statistics. The most general third-order statistics in configuration space is the three-point correlation or its reduced counter part (Groth and Peebles 1977). In this subsection we describe our bias measurements from paper I, which are derived from the symmetrized reduced three-point halo-matter-matter cross-correlation in configuration space (hereafter referred to as 3pcc, see also Pollack et al. 2012). It is defined as

$$Q^\times \equiv \frac{1}{3} \frac{\zeta^{hmm} + \zeta^{mhm} + \zeta^{mmh}}{\zeta_H^{hm}}, \quad (8)$$

where

$$\zeta^{xyz} \equiv \langle \delta_{x,1} \delta_{y,2} \delta_{z,3} \rangle \quad (9)$$

is the three-point halo-matter-matter cross-correlation and

$$\zeta_H^{hm} \equiv \xi_{12}^{hm} \xi_{13}^{hm} + \xi_{12}^{mh} \xi_{23}^{hm} + \xi_{13}^{mh} \xi_{23}^{mh} \quad (10)$$

is the corresponding hierarchical three-point cross-correlation. The average  $\langle \dots \rangle$  is made over triangles of any orientation and position. The auto-correlation for halo and matter density fields ( $Q_h$  and  $Q_m$  respectively) are defined analogously and will be referred to as 3pc in the following. For measuring the bias accurately using the 3pcc one needs to take into account non-local contributions to the bias function. A neglect of the latter would cause a  $\sim 20\%$  error in the estimation of the linear bias parameter (see Manera and Gaztañaga 2011; Chan et al. 2012; Baldauf et al. 2012). We therefore proposed in paper I to measure the linear bias independently of quadratic

local and non-local contributions by combining three-point auto- and cross-correlations,

$$b_{\Delta Q} \equiv -2 \frac{Q_m}{Q_h - 3Q_h^\times}. \quad (11)$$

A similar combination of auto- and cross-correlations allows for the determination of the quadratic local and non-local bias parameters ( $c_2$  and  $\gamma_2$ ) independently of  $Q_m$ , once the linear bias is determined (for instance via equation (11) or the 2pc),

$$\Delta Q_{cg} \equiv Q_h - Q^\times = \frac{2}{3} \frac{1}{b_1} [c_2 + g_2 Q_{nloc}]. \quad (12)$$

We predict the non-local contribution  $Q_{nloc}$  from the non-linear power spectrum, which has been measured in the simulation. Details on this prediction are provided in the appendix of paper I. Combining three-point auto- and cross-correlation for measuring bias will be referred to as  $\Delta Q$  method in the following. The results in this work are derived from 3pc measurements which are computed using triangles with fixed legs of 36 and  $72h^{-1}\text{Mpc}$  at 18 opening angles between these legs. The density fields were smoothed with an  $8h^{-1}\text{Mpc}$  Top-hat window function, and the covariance between measurements at different opening angles was estimated from 64 JK samples. Details on these measurements are presented in paper I, where we also study the dependence of 3pc bias measurements on the triangle scale.

### 3.4 third-order cross-moments

Alternatively to the 3pc one can explore the third-order statistical properties of comic fields with 1- and 2-point statistics. Despite the fact that they do not provide access to the full third-order hierarchy probed by the 3pcc (Subsection 3.3) they are useful tools for comparing the statistical properties of the halo distribution with respect to the underlying matter field.

These 1- and 2-point statistics correspond to the 3pc for very specific triangle configurations. The 3pc for triangles which are collapsed into two points corresponds to the correlator  $C_{12}$  (see Bernardeau 1996), while for a further collapse into a single point yields the skewness  $S_3$  (see Bernardeau et al. 2002). As in case of the 3pcc, it is possible to define the cross-skewness  $S_{3,h}^\times$  and the cross-correlator  $C_{12,h}^\times$  as

$$S_{3,h}^\times \equiv \frac{\langle \delta_h \delta_m^2 \rangle}{\langle \delta_h \delta_m \rangle^2} \quad (13)$$

and

$$C_{12,h}^\times \equiv \frac{\langle \delta_{h,1} \delta_{h,2} \delta_{m,2} \rangle}{\langle \delta_{h,1} \delta_{h,2} \rangle \langle \delta_h \delta_m \rangle} \quad (14)$$

where  $\delta_h$  and  $\delta_m$  are respectively the density contrast of halo and matter density fields which are smoothed with a spherical top-hat window function of radius  $R$ . The auto skewnesses  $S_{3,h}$  and  $S_3$  and the auto-correlators  $C_{12,h}$  and  $C_{12}$  for halo and matter density fields respectively are defined analogously. We provide details on how we measure these quantities and how to correct them for shotnoise in paper I.

One can express the linear and quadratic bias parameters independently from each other using the combinations

$$b_\tau^\times \equiv \frac{S_3 - C_{12}}{S_{3,h}^\times - C_{12,h}^\times} \equiv \frac{\tau^\times}{\tau_h^\times} \quad (15)$$

and

$$c_\tau^\times \equiv \frac{S_3 C_{12,h}^\times - C_{12} S_{3,h}^\times}{\tau_h^\times}. \quad (16)$$

We will refer to this way of measuring bias as the  $\tau^\times$ -method in the following. For spherically averaged quantities such as skewness, correlators, cross-skewness and cross-correlators non-local contributions of the second order described by equation (4) lead to an effective second-order local bias

$$c_2^{\text{eff}} = c_2 - \frac{4}{3} \frac{\gamma_2}{b_1}, \quad (17)$$

but do not affect the estimated linear bias parameter  $b_1$  unless for highly biased samples (M3, see discussion in paper I). The same effect has been pointed out by Chan et al. (2012) for the  $\delta_g - \delta_m$  method for measuring bias, which is described in Section 3.1. Assuming a local lagrangian bias model,  $\gamma_2 = -\frac{2}{7}(b_1 - 1)$  we expect the non-local contributions to  $c_2^{\text{eff}}$  to be zero for  $b_1 = 0$  and  $\lesssim 0.3$  for  $b_1 = 4$ . However these expectation will not be accurate as moderate deviations from the lagrangian bias model have been reported by Chan et al. (2012) and in paper I.

### 3.5 Peak-background split predictions

The peak-background split (hereafter referred to as PBS) model provides predictions for the linear and non-linear bias parameters as a function of the halo mass, which are deduced from derivatives of the mass function. Model fits to mass function measurements therefore provide analytical expression of the bias as a function of halo mass.

Such PBS bias predictions are essential for various purposes like bias modeling as function of galaxy properties via Halo Occupation Distribution (HOD) modelling, cluster mass calibration or predictions of the cluster count and power spectra covariances (e.g. Cooray and Sheth 2002; Lima and Hu 2004, 2005; Lacasa and Rosenfeld 2016). It is therefore important to verify how accurate the PBS model is able to predict bias measurements in simulations.

In the present analysis we validate the accuracy of PBS predictions for the linear, quadratic and third-order bias parameters by comparing them to the various measurements described in the previous subsections.

We employ fits to the mass function measured in the MICE-GC simulation, using the models of Tinker et al. (2010) and Warren et al. (2006) as well as a new model presented in paper II. The sample M0 is excluded from the fitting range since we expect halo detection in the corresponding mass range to be very noisy, as we discuss in paper II. However, the predictions can still be made over the full mass range for all the samples M0-M3.

## 4 RESULTS

### 4.1 bias comparison

We compare in Fig. 1 the linear and non-linear bias parameters from the different measurements and the PBS predictions described in Section 3 using the mass samples M0-M3 (defined in Table 2) at the redshifts  $z = 0.0$  and  $z = 0.5$ .

#### 4.1.1 linear bias

In the case of the linear bias ( $b_1$ , top panel of Fig. 1) we find an overall variation of roughly 5 percent between results from different measurements and PBS predictions at all masses and both redshifts. The measurements from the 2pcc ( $b_\xi^\times$ , equation (7)) are expected to be the most reliable estimate with percent level accuracy (see e.g. paper I). We therefore use it as a reference for evaluating the accuracy of the other linear bias measurements and predictions in our comparison.

The results in Fig. 1 show that both estimations for the linear bias from third-order statistics, ( $\Delta Q$  and  $\tau^\times$ , described in Section 3.3 and 3.4 respectively) are in  $1\sigma$  agreement with  $b_\xi^\times$ . However, the errors of  $b_\tau^\times$  are roughly 10 percent, while those of  $b_{\Delta Q}$  at the one percent level. We attributed the strong deviation of  $b_\tau^\times$  from all other results at high masses to an inadequate shot-noise corrections in paper I. From the same analysis we expect larger deviations from  $b_\xi^\times$  when the linear bias is measured from third-order auto- instead of cross-correlations correlations and when non-local contributions are not taken into account.

The linear bias measurements from the  $\delta_h - \delta_m$  method (described in Section 3.1) are both in percent level agreement with  $b_\xi^\times$  which is consistent with results from Manera and Gaztañaga (2011) or Pollack et al. (2012). Results from the  $\delta$ PDF method tend to be overall slightly larger with  $\lesssim 7\%$  deviations from  $b_\xi^\times$ . Possible reasons for the discrepancies can be the truncation of the bias function at third order (see discussion in Section 3.1) or inaccuracies in the covariance estimation from Jackknife sampling, which can affect the best fit values.

In addition to the bias measurements we show predictions from the PBS model, which are based on different MICE-GC mass function fits from paper II. The different predictions show a very good mutual agreement in the mass range spanned by the samples M1-M3 which was used for the fits. For the low mass sample, which was excluded from the fitting range due to noisy halo detection, the different PBS predictions show a stronger variation. For the mass samples M2 and M3 ( $\gtrsim 10^{13} h^{-1} M_\odot$ ) all predictions lie up to  $\sim 7$  percent below  $b_\xi^\times$ , which is consistent with findings in the literature (e.g. Manera et al. 2010; Manera and Gaztañaga 2011; Pollack et al. 2012). The agreement between predictions from different mass function fits indicates that the inaccuracy of PBS bias is driven by shortcomings of the model, rather than uncertainties in the fits. A more detailed comparison between  $b_\xi^\times$  and these PBS predictions has been presented and discussed in paper II.

**Table 3.** Bias estimators, definitions and notations. The term cross refers to halo-matter cross correlations,  $b$  and  $c$  indicate linear and non-linear bias estimations respectively.

	method	bias parameters	reference
measurements	$\delta_h - \delta_m$ relation	$b_1, c_2, c_3$	Section 3.1, Appendix A
	PDF of $\delta_h$ and $\delta_m$	$b_1, c_2, c_3$	Section 3.1, Appendix A
	2-point cross-correlation $\xi^\times$	$b_1$	Section 3.2, paper I
	combination of 3-point auto- and cross-correlations $\Delta Q$	$b_1, c_2$	Section 3.3, paper I
	3rd-order cross-moments $\times^\times$	$b_1, c_2$	Section 3.4, paper I
predictions	peak-background split (PBS) model	$b_1, c_2, c_3$	Section 3.5, paper II

#### 4.1.2 non-linear bias

Measurements and prediction of the second- and third-order bias parameters ( $c_2 \equiv b_2/b_1$  and  $c_3 \equiv b_3/b_1$ ) are shown in the central and bottom panels of Fig. 1 respectively. Note that for this comparison we do not have a reference for the non-linear bias, which would require separate universe simulations. Furthermore our measurements from third-order statistics provide only bias parameters up to second order, since they are based on leading order perturbation theory. Measurements of  $c_3$  are therefore only obtained from the  $\delta_h - \delta_m$  relation. Overall we find a stronger variation between the different results for the non-linear bias than for the linear bias. Yet, all the different non-linear bias measurements and predictions show similar mass dependencies at both redshifts.

The second-order bias  $c_2$  depends only weakly on the halo mass below  $\lesssim 10^{13} h^{-1} M_\odot$  (covered by the mass samples M0 and M1), with a value of  $\simeq -0.5$  at both redshifts. In the mass range  $\simeq 10^{13} - 10^{14} h^{-1} M_\odot$ , which corresponds to the mass sample M2,  $c_2$  changes from negative to positive values, and increases rapidly with mass to values of up to 2 at  $z = 0.5$  for halo masses of higher than  $10^{14} h^{-1} M_\odot$ . The PBS prediction for  $c_2$  from all mass function fits show an overall smaller mass dependence than the corresponding measurements, as the former lie above the results from the  $\Delta Q$ ,  $\tau^\times$  and  $\delta_h - \delta_m$  methods in the mass range spanned by M0-M2, where  $c_2$  is negative. For the high mass sample M3, where  $c_2$  is positive at both redshifts we find the opposite. The latter result confirms findings of Manera and Gaztañaga (2011) on a larger mass range. In the mass range M0-M2 the measurements from the  $\Delta Q$ ,  $\tau^\times$  and  $\delta_h - \delta_m$  methods agree mutually at the  $1\sigma$  level at both redshifts, while results vary strongly for the high mass sample M3. Note that we expect the  $c_2$  measurements from the  $\delta_h - \delta_m$  and  $\tau^\times$  to be biased by non-local contributions with values between zero for  $b_1 = 0$  and  $\lesssim 0.3$  for  $b_1 = 4$ , as discussed in Section 3.4, which is comparable with the variation among the different results.

In the bottom panel of Fig. 1 we present a validation of third-order bias prediction from the PBS model with direct measurements from the  $\delta_h - \delta_m$   $\delta$ PDF methods. The predictions and measurements are in an overall agreement with each other, as both decrease from positive values of around unity for M0 to negative values of down to  $\lesssim -3$  for M3 at both redshifts. The zero crossing of  $c_3$  occur between  $10^{12.5} - 10^{13.5} M_\odot/h$ . Overall the predictions tend to be smaller than the measured values.

## 4.2 Universal relation between bias parameters

Our various bias measurements enable us to validate the universal relation between the linear and non-linear bias parameters  $b_2(b_1)$  and  $b_3(b_1)$ , which we found for PBS predictions and linear bias values of  $b_1 \gtrsim 2$  in paper II.

In Fig. 2 we show the linear bias versus the quadratic and third-order bias parameters from the different measurements together with the PBS predictions for redshift  $z = 0.0$  and  $0.5$ . We find overall consistent results from measurements and predictions which also line up with results from Lazeyras et al. (2015). These authors obtained their bias measurements using separate universe simulations in combination with the PBS model and demonstrated together with Baldauf et al. (2015) and Li et al. (2015), that their linear bias obtained from this method is in very good agreement with measurements from two-point statistics. It is interesting to note that their  $b_2(b_1)$  relation agrees best with our measurements derived from the  $\Delta Q$  method, since the latter also delivers very accurate measurements of the linear bias. This suggests that also the  $c_2$  measurements and hence the  $b_2 - c_2$  relations from these two approaches are reliable. Furthermore we include bias measurements from Chan et al. (2012), which are based on the Bispectrum and find a good agreement with our results.

The fact that predictions as well as measurements for the  $b_N(b_1)$  relations from simulations with different cosmologies and results from different redshifts are similar to each other indicate a roughly universal behaviour between the linear and higher-order bias parameters

Fitting a the polynomial

$$b_N = \sum_{n=0}^{N=2} \alpha_n b_1^n \quad (18)$$

to our  $b_2(b_1)$  measurements from  $\Delta Q$  we find  $(\alpha_0, \alpha_1, \alpha_2) = (0.77, -2.43, 1)$ .

## 5 SUMMARY AND CONCLUSION

This analysis is the last part of a series of articles on the accuracy of halo bias parameters derived from the MICE Grand Challenge (MICE-GC) simulation using clustering statistics and peak-background split (referred to as PBS) predictions (Hoffmann et al. 2015b, paper I, paper II). In the present analysis we studied bias parameters derived from the relation between matter and halo density contrasts ( $\delta_h, \delta_m$  respectively) as an additional method for measuring bias and compare these measurements to a selection of our most robust previous results.

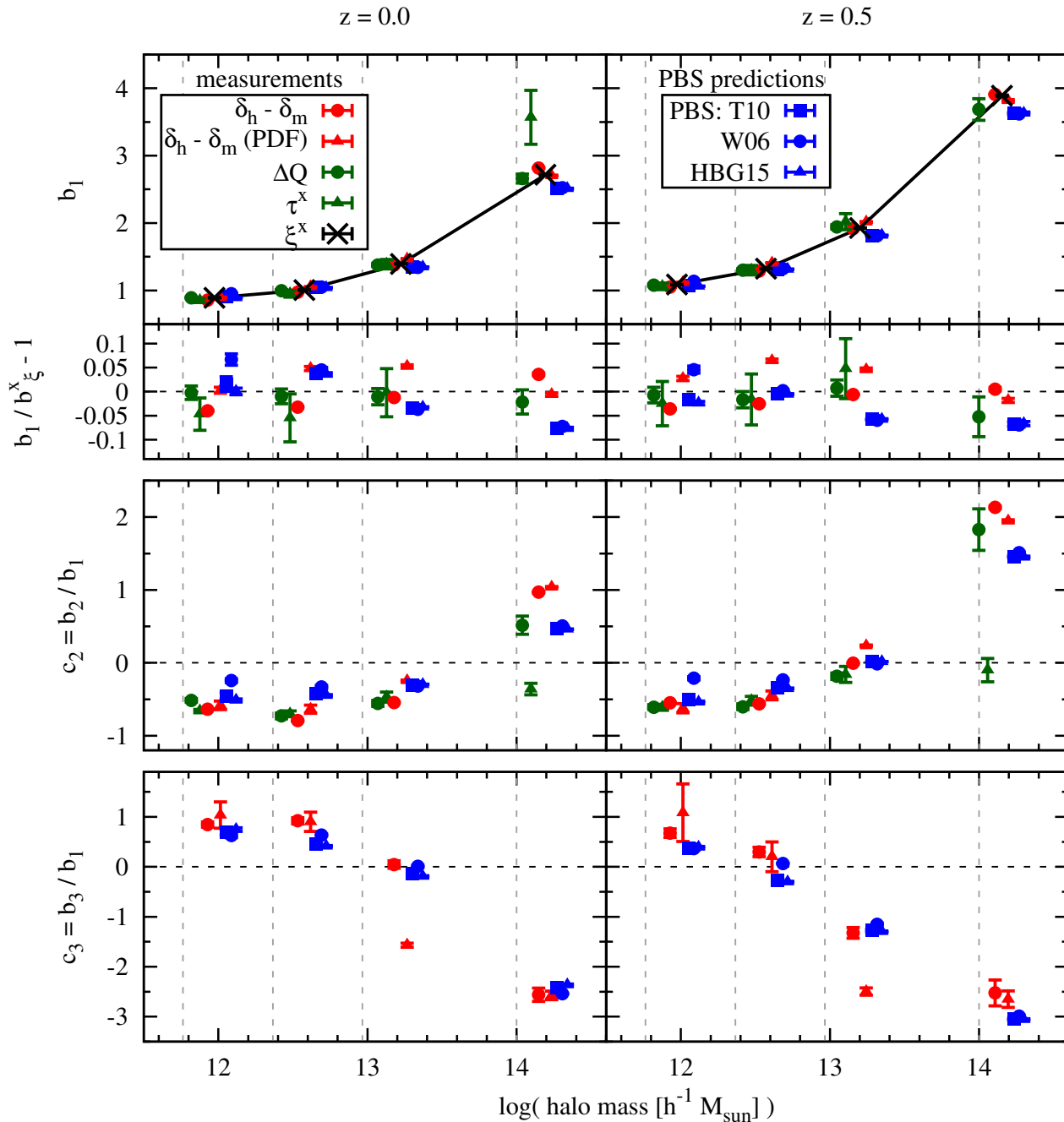


**Figure 1.** Summary of various bias measurements from second- and third-order halo-matter cross-correlations ( $\xi^\times$ ,  $\Delta Q$  and  $\tau^\times$ ),  $\delta_h - \delta_m$  relations and PBS predictions, described in Section 3. The top, central and bottom panel show the first- second- and third-order bias parameters respectively at  $z = 0.0$  and  $0.5$  (left and right panel) versus the mean halo mass of each mass samples M0-M3 (slightly shifted along the mass axis for clarity). The subpanel at the bottom of the top panel shows relative deviations from  $\xi^\times$ . The lower and upper limits of the mass samples are marked by vertical grey dashed lines. Error bars denote  $\sigma$  uncertainties.

In particular these previous results are derived from two-point halo-matter cross-correlations ( $\xi^\times$ ), a combination of three-point halo-matter auto- and cross-correlations ( $\Delta Q$ ) as well as a combination of the halo-matter cross-skewness and cross-correlators ( $\tau^\times$ ). We thereby employ leading-order modeling of clustering statistics, at which the linear bias parameters from these estimators are not affected by non-local contributions to the bias model. We therefore

obtain the linear bias from  $\xi^\times$  and the linear and quadratic bias from  $\Delta Q$  and  $\tau^\times$ . The PBS predictions are based on MICE-GC mass function fits from paper II, using different mass function models, while we study bias parameters up to order three, for which we have corresponding measurements from the  $\delta_h - \delta_m$  relation for validation.

We studied in this work bias measurements from the  $\delta_h - \delta_m$  relation in two ways. The more common method

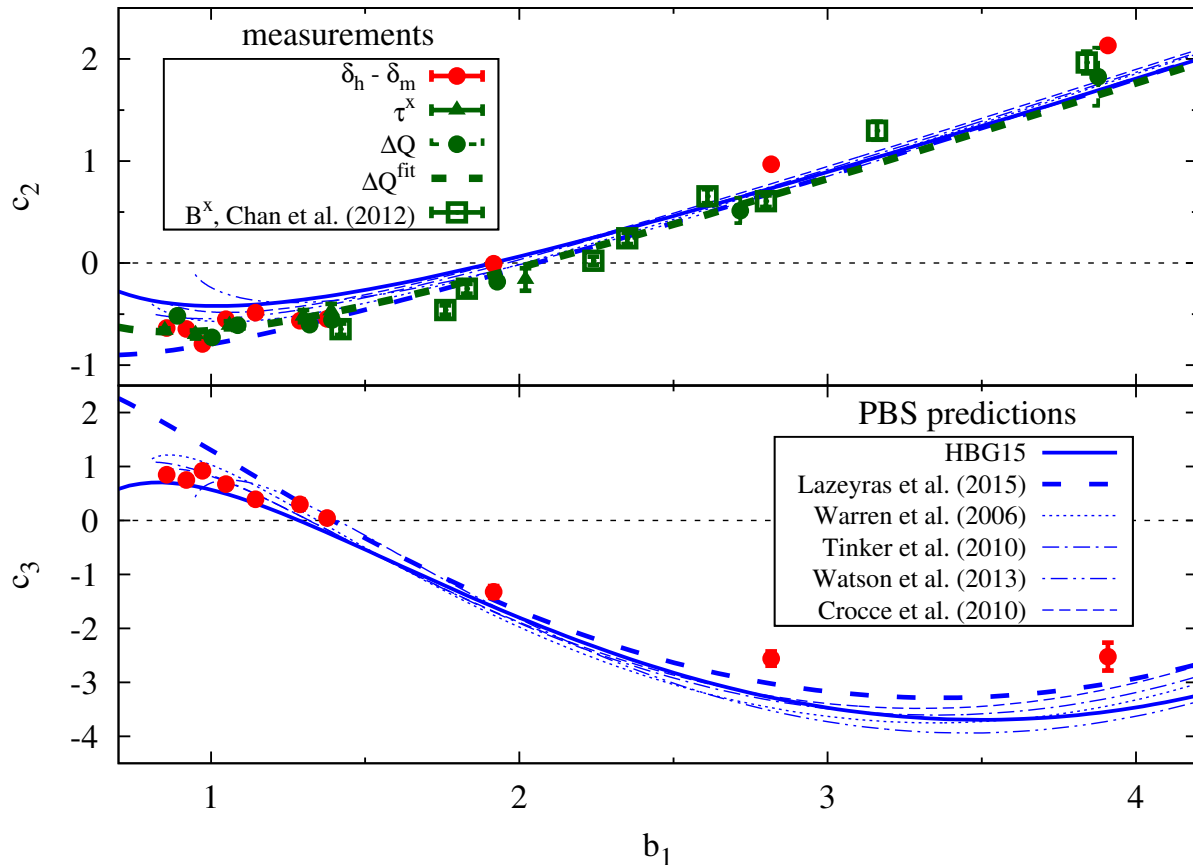


**Figure 2.** Second- and third-order bias parameters versus the linear bias parameter  $b_1$  (top and bottom panel respectively). Results from  $\Delta Q$  and  $\tau^\times$ ,  $\delta_h - \delta_m$  as well as PBS predictions from HBG15 are the same as those shown in Fig. 1. In addition we show PBS prediction based on mass function fits from the literature. Fits to the  $b_1 - c_1$  and  $b_1 - c_3$  relations from separate universe simulations in combination with the PBS model, given by Lazeyras et al. (2015) are shown as long dashed blue lines.

is to fit a polynomial to the  $\delta_h - \delta_m$  relation, measured in the simulation. Alternatively we explore bias measurements obtained from the probability distribution function (referred to as PDF) of  $\delta_h$  and  $\delta_m$ . The latter method has the advantage that it can be directly applied to observations, since the PDF of matter density contrasts can be modelled with theory or simulations (Bel et al. 2016; Di Porto et al. 2014; Marinoni et al. 2005; Bernardeau et al. 2002). However, it has not been tested so far how accurately the bias parameters can be determined with this method.

The results of our bias comparison are summarized in Fig. 1. In the case of the linear bias  $b_1$  we consider results from  $\xi^\times$  ( $b_\xi^\times$ ) as the most reliable since non-linear local and non-local term can safely be neglected. Furthermore,  $b_\xi$  is highly relevant for cosmology since it is weakening constraints on cosmological parameters inferred from  $\xi$  due to its degeneracy with the growth of matter fluctuations.

Linear bias measurements and predictions from all other methods are in a  $\sim 5$  percent agreement with  $b_\xi^\times$ , while  $\Delta Q$  delivers the most accurate measurements with an overall percent level accuracy. Standard measurements from the  $\delta_h - \delta_m$  relation are in a slightly better overall agreement with  $b_\xi^\times$  than those from the  $\delta$ PDF-method. The strongest deviations from  $b_\xi^\times$  shows the linear bias predictions from the different PBS model. These predictions are consistently

up to 7 percent below  $b_\xi^\times$  at high masses as reported in the literature (e.g. Manera and Gaztañaga 2011; Pollack et al. 2012). We do not find a clear change of the variation between the different measurements and predictions with mass or redshift.

In the case of the quadratic bias  $c_2 \equiv b_2/b_1$  we find consistent results from the different measurements and predictions as  $c_2$  increases from negative values of  $\gtrsim -0.5$  at low halo masses ( $\sim 10^{12} M_\odot/h$ ) to positive values of up to  $\sim 2$  at high masses ( $\gtrsim 10^{14} M_\odot/h$ ). However, the variation between the different results tends to be larger than in the case of  $b_1$ . In the case of the measurements this effect is presumably caused by the strong assumptions such as the validity of tree-level perturbation theory ( $\Delta Q$  and  $\tau^\times$ ), Poissonian shot-noise ( $\tau^\times$ ), or a local deterministic bias model ( $\delta_h - \delta_m$ ). We therefore do not consider any of these measurements to be sufficiently reliable for being a reference, such as the results from  $\xi^\times$  in the case of the linear bias. However, the fact that the  $\Delta Q$  method delivers highly accurate measurements of the linear bias suggests that also the quadratic bias is measured reliably with this approach. We find the PBS predictions for  $c_2$  to be consistently above (below) all measurements in the low (high) mass range as they show overall weaker mass dependence. The latter finding lines up with re-

ports from Manera and Gaztañaga (2011) and Pollack et al. (2012).

Both measurements of the third-order bias  $c_3 \equiv b_3/b_1$  from the  $\delta_h - \delta_m$  relation agree overall mutually at the  $1\sigma$  level. These measurements allow for a validation of the corresponding PBS predictions. Results from both methods are similar as  $c_3$  is positive below unity in the low mass range and decreases to negative values of down to  $\sim -3$  in the high masses range. However, deviations are significant, as the PBS predictions tend to be below the measurements at low halo masses while results based on different mass function fits are consistent with each other.

We use our various linear and non-linear bias measurements for validating the universal polynomial relation between linear and non-linear bias ( $b_2(b_1)$  and  $b_3(b_1)$ ), which we deduced in paper II from PBS predictions. Our measurements agree with the universal behaviour predicted by the PBS model. Furthermore they agree with results from the literature derived via the Bispectrum in Fourier space or the separate universe approach from simulations with cosmologies different to the one of MICE (i.e. Chan et al. 2012; Lazeyras et al. 2015). We fit a second-order polynomial to  $b_2(b_1)$  measurements from  $\Delta Q$ , which we consider as the most reliable  $c_2$  estimator as mentioned above.

Such a universal relation between linear and non-linear bias can be useful for reducing errors on the linear bias and the growth from clustering analysis when the latter is affected by  $c_2$ , for instance in the case of three-point correlations or two-point correlations at small scales.

For applying universal polynomial relations between bias parameters in the analysis of galaxy surveys it would be interesting to show that their universality also holds for halo samples, which are selected by galaxy properties, such as luminosity and colour instead of halo mass. A correlation between the linear and quadratic bias from the 3pc and Bispectra has been reported by for SDSS galaxy samples and mock HOD catalogues by Kayo et al. (2004) and Nishimichi et al. (2007) and compared with PBS predictions. The limited accuracy of their measured  $b_1 - c_2$  relations could be strongly improved using the methods studied in the present analysis in combination with data from upcoming galaxy surveys.

## ACKNOWLEDGEMENTS

Funding for this project was partially provided by the Spanish Ministerio de Ciencia e Innovacion (MICINN), project AYA2009-13936, Consolider-Ingenio CSD2007-00060, European Commission Marie Curie Initial Training Network CosmoComp (PITN-GA-2009-238356) and research project 2009- SGR-1398 from Generalitat de Catalunya. KH is supported by beca FI from Generalitat de Catalunya and ESP2013-48274-C3-1-P. He also acknowledges the Centro de Ciencias de Benasque Pedro Pascual where parts of the analysis were done. The MICE simulations have been developed by the MICE collaboration at the MareNostrum supercomputer (BSC-CNS) thanks to grants AECT-2006-2-0011 through AECT-2010-1-0007. Data products have been stored at the Port d'Informaci Cientfica (PIC).

We thank Martin Crocce, Pablo Fosalba, Francisco

Castander and Roman Scoccimarro for interesting and useful comments.

## References

- Baldauf T., Seljak U., Desjacques V., McDonald P., 2012, Phys.Rev.D, 86, 083540
- Baldauf T., Seljak U., Senatore L., Zaldarriaga M., 2015, ArXiv e-prints
- Bel J., Hoffmann K., Gaztañaga E., 2015, MNRAS, 453, 259
- Bel J., et al., 2016, A&A, 588, A51
- Bernardeau F., 1996, A&A, 312, 11
- Bernardeau F., Colombi S., Gaztañaga E., Scoccimarro R., 2002, Phys. Rept., 367, 1
- Chan K.C., Scoccimarro R., Sheth R.K., 2012, Phys.Rev.D, 85, 083509
- Chang C., et al., 2016, MNRAS
- Colombi S., 1994, ApJ, 435, 536
- Cooray A., Sheth R., 2002, Phys. Rept., 372, 1
- Crocce M., Castander F.J., Gaztanaga E., Fosalba P., Carretero J., 2013, ArXiv e-prints
- Davis M., Efstathiou G., Frenk C.S., White S.D.M., 1985, ApJ, 292, 371
- Di Porto C., et al., 2014, ArXiv e-prints
- Fosalba P., Crocce M., Gaztanaga E., Castander F.J., 2013, ArXiv e-prints
- Fry J.N., Gaztanaga E., 1993, ApJ, 413, 447
- Gaztañaga E., Fosalba P., Elizalde E., 2000, ApJ, 539, 522
- Groth E.J., Peebles P.J.E., 1977, ApJ, 217, 385
- Hoffmann K., Bel J., Gaztañaga E., 2015a, MNRAS, 450, 1674
- Hoffmann K., Bel J., Gaztañaga E., Crocce M., Fosalba P., Castander F.J., 2015b, MNRAS, 447, 1724
- Kayo I., et al., 2004, PASJ, 56, 415
- Lacasa F., Rosenfeld R., 2016, ArXiv e-prints
- Lazeyras T., Wagner C., Baldauf T., Schmidt F., 2015, ArXiv e-prints
- Li Y., Hu W., Takada M., 2015, ArXiv e-prints
- Lima M., Hu W., 2004, Phys.Rev.D, 70, 043504
- Lima M., Hu W., 2005, Phys.Rev.D, 72, 043006
- Manera M., Gaztañaga E., 2011, MNRAS, 415, 383
- Manera M., Sheth R.K., Scoccimarro R., 2010, MNRAS, 402, 589
- Marinoni C., et al., 2005, A&A, 442, 801
- Nishimichi T., Kayo I., Hikage C., Yahata K., Taruya A., Jing Y.P., Sheth R.K., Suto Y., 2007, PASJ, 59, 93
- Pollack J.E., Smith R.E., Porciani C., 2012, MNRAS, 420, 3469
- Pujol A., et al., 2016, ArXiv e-prints
- Springel V., 2005, MNRAS, 364, 1105
- Tinker J.L., Robertson B.E., Kravtsov A.V., Klypin A., Warren M.S., Yepes G., Gottlöber S., 2010, ApJ, 724, 878
- Wagner C., Schmidt F., Chiang C.T., Komatsu E., 2015, MNRAS, 448, L11
- Warren M.S., Abazajian K., Holz D.E., Teodoro L., 2006, ApJ, 646, 881

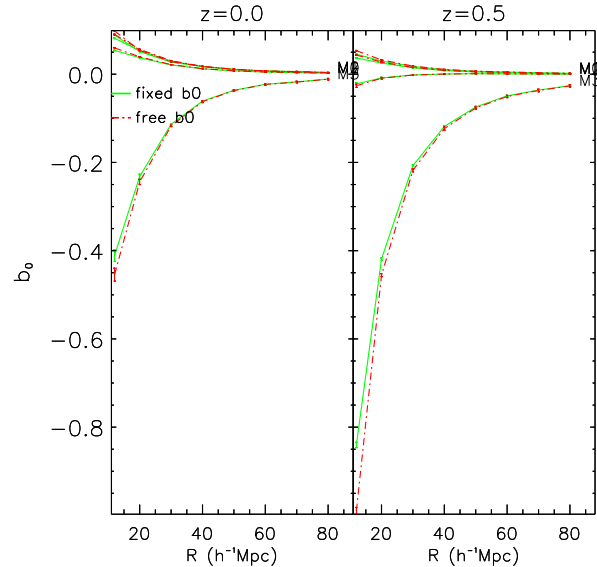
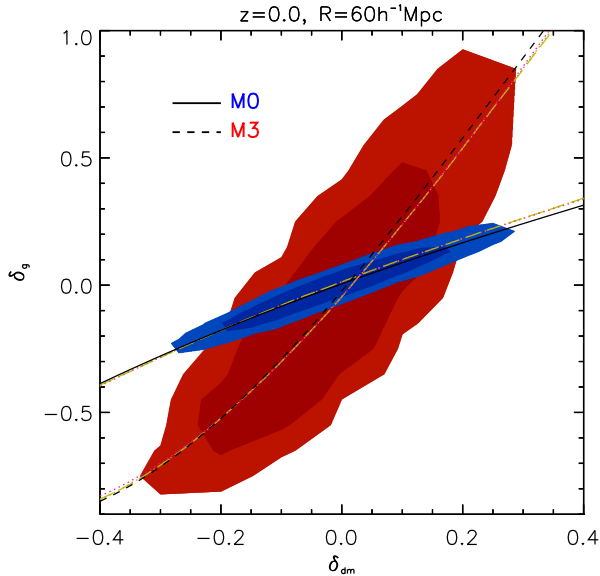


**Figure A1.** Scatter plot between halo and matter density contrast at  $z = 0.5$  (*top*) and  $z = 0$  (*bottom*) obtained with a smoothing radius  $R = 60h^{-1}\text{Mpc}$ . In each panel we represent the 68% (Dark) and 95% (Light) contour levels, in red we show the contour levels corresponding to the mass bin M3 and in blue we show the mass bin M0. **Black dashed lines show the bias function derived from the  $\delta_h - \delta_m$  method, while the green and red and magenta lines show results from variants of the  $\delta PDF$  method (see text for details).**

## APPENDIX A: BIAS PARAMETERS FROM THE $\delta_H - \delta_M$ RELATION

The scatter between halo and matter density contrasts in the MICE-GC simulation is shown in Fig. A1 at redshift  $z = 0.0$  for a smoothing scale of  $R = 60h^{-1}\text{Mpc}$ . Given the expression of the biasing function in equation (2), we obtain an estimator of the halo bias coefficients  $b_i$  by fitting a third-order polynomial to the scatter plot.

Fig. A2 and A3 show the results of this fitting process for respectively  $b_0$ ,  $b_1$  and  $c_2$ ,  $c_3$  when applied at various smoothing scale  $R$ . For each scale, we estimate the error by performing the fit in 64 Jackknife sub-samples of the full simulation. Examination of the top panel of Fig. A2 shows that  $b_0$  changes with scale, while converging to zero. Furthermore its sign depends on the mass of the halo sample. Both effects are expected because  $b_0$  must be chosen in order to ensure that the average of the density contrast is zero (i.e.  $\langle \delta_h \rangle = 0$ ). This condition leads to its formal expression with respect to the dark matter cumulant moments

$$b_0 = -b_1 \sigma_{dm}^2 \left\{ \frac{c_2}{2} + \frac{c_3}{6} S_{3,dm} \sigma_{dm}^2 \right\}, \quad (\text{A1})$$

where  $S_{3,dm}$  is the Skewness of the dark matter field. As shown by equation (A1) the sign of  $b_0$  can change, depending on the second- and third-order bias coefficients. Moreover, the dependence of  $b_0$  on scale can be expected since it depends on scale dependent quantities such as the variance  $\sigma_{dm}^2$  and Skewness  $S_{3,dm}$ . We compared two ways of proceeding when measuring bias parameters from the  $\delta_h - \delta_m$  relation. We either fix  $b_0$  using equation (A1) or consider it

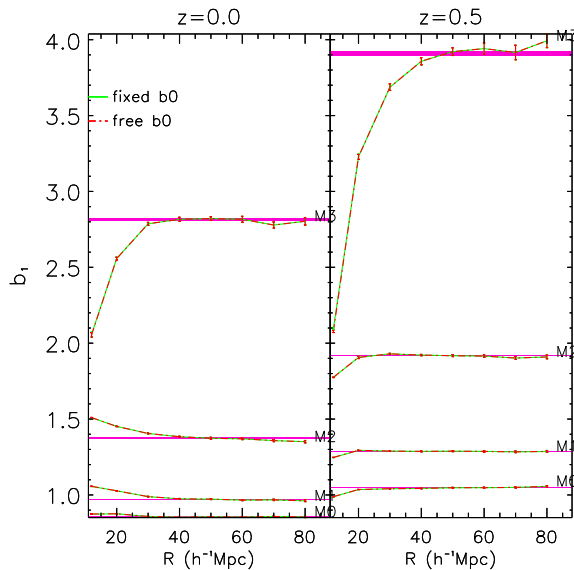


**Figure A2.** *Top:* Constant bias coefficient  $b_0$ . *Bottom:* Linear bias coefficient  $b_1$ . In all panels, we estimate quantities by letting vary the smoothing scale  $R$ . We adopt two methods, in the first we fix  $b_0$  (green solid line) using equation A1 and in the second we allow  $b_0$  to vary as a free parameter (red dashed line). In the bottom panel we also represented the results of the fit between  $40h^{-1}$  and  $80h^{-1}\text{Mpc}$ . We perform this analysis for two comoving outputs at redshift 0 (left) and 0.5 (right).

as an additional free parameter (green solid and red dashed lines respectively in Fig. A2 and A3). This allows to be more confident in the estimation of the other bias parameter, when the linear regime is reached the two approaches must give the same value for the  $b_0$  parameter (see smoothing radius larger than  $40h^{-1}\text{Mpc}$  in the top panel of Fig. A2). Note that another possible source of discrepancy could be the shot noise, which we do not take into account.

However, the consistency between the bias coefficients  $b_1$  (bottom panel of Fig. A2),  $c_2$  and  $c_3$  (top and bottom panel of Fig. A3), obtained from these two methods, indic-

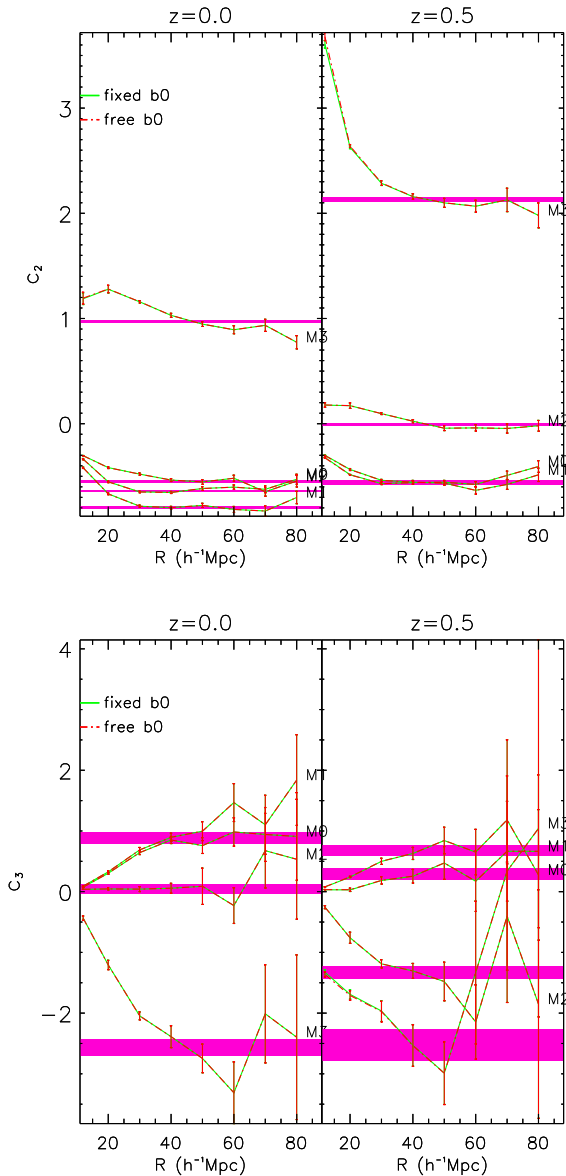


**Figure A3.** *Top:* Contant bias coefficient  $b_0$ . *Bottom:* Linear bias coefficient  $b_1$ . In all panels, we estimate quantities by letting vary the smoothing scale  $R$ . We adopt two methods, in the first we fix  $b_0$  (green solid line) using equation A1 and in the second we allow  $b_0$  to vary as a free parameter (red dashed line). We also represented the results of the fit between  $40h^{-1}$  and  $80h^{-1}\text{Mpc}$ . We perform this analysis for two comoving outputs at redshift 0 (left) and 0.5 (right).

ates that the shot noise contribution has a small influence on the estimation of the bias parameters, even at small scales.

The results displayed in Fig. A2 and A3 show that on small scales the higher-order coefficients present an important scale dependence (see also Manera and Gaztañaga 2011) but still converge on large scales ( $\gtrsim 40 h^{-1}\text{Mpc}$ ) to a constant value. We therefore use the values measured between  $R = 40$  and  $80 h^{-1}\text{Mpc}$  to fit a constant for each coefficient which is referred to, in this article, as  $\delta_h - \delta_h$  estimator. Note that we take into account any possible correlation between

bias measurements at different scales by estimating the covariance matrix with Jackknife sub-sampling.

An alternative way of measuring the bias parameters is to match the 1-point probability distribution of haloes and matter fluctuations ( $P_h(\delta_h)$  and  $P_m(\delta_m)$  respectively)

$$C_h[\delta_h] = C_m[\delta_m], \quad (\text{A2})$$

where  $C_i$  is the cumulative distribution function, defined as  $C_i[\delta_i] \equiv \int_{-1}^{\delta_i} P_i(\delta'_i) d\delta'_i$  for either haloes ( $i = h$ ) or matter ( $i = m$ ). The halo density fluctuations  $\delta_h$  can thus be expressed as a function of halo density fluctuations  $\delta_m$  by inverting equation (A2) (i.e.  $\delta_h(\delta_m) = C_h^{-1}[C_m[\delta_m]]$ ), which is by definition the local bias function. The exponent  $-1$  denotes the reciprocal function. The mapping  $C_h C_m^{-1}$  is obtained by integrating numerically the probability distribution function of both the halo and matter density contrasts. We use a cubic smoothing of size  $64h^{-1}\text{Mpc}$  which corresponds in volume to a spherical smoothing of radius  $R \simeq 40h^{-1}\text{Mpc}$ . Note that when the average number of haloes per cell is smaller than 150, it is necessary to correct from shot noise effects (see Di Porto et al. 2014). In order to reconstruct the PDF of haloes/galaxies (this is indeed the case for M2 and M3 samples) we use that the discrete probability distribution  $P_N$  (where  $N$  represents the number of haloes inside a cell) is related to the probability density function of matter fluctuations via

$$P_N = \int_{-1}^{\infty} K[N|\bar{N}(1 + \delta_h)] P_h(\delta_h) d\delta_h, \quad (\text{A3})$$

where  $K$  is the conditional sampling probability which we assume to be a Poisson distribution. In practice the inversion of equation (A3) requires some subtleties (see Bel et al. 2016). We apply three different methods and choose the one which provides us with the best description of the counting probability distribution  $P_N$ . Given the high shot noise level in the M2 and M3 samples we assume a parametric form for the density probability  $P_h$ , in practice we tested a skewed-LogNormal (Colombi 1994) and a Gamma expansion (Gaztañaga et al. 2000) and found that the Gamma expansion offers a better matching of the measured counting probabilities.

Once we obtain the bias function we devised two ways of estimating the bias parameters. In both cases we fix an effective range on which the Taylor expansion must be valid and on one hand we fit the bias function with a polynomial of order three (referred to as *proba. 1*) and on the other hand we apply discrete derivatives method (referred to as *proba. 2*). We allow the effective range in  $\delta$  to decrease and stop when the two methods converge to the same values for  $b_1$ ,  $c_2$  and  $c_3$ . An illustration of this technique is displayed in Fig. A1, where we show in green long dashed line the bias function obtained from inversion of equation (A2) together with the Taylor expansion estimated from the fitting method (orange dotted line) and from the numerical derivatives method (magenta dotted line) One can see that on one hand the result from the two methods agrees well with the obtained bias function from the probability density function and on the other hand we can see some significant departures from the Taylor expansion obtained from the direct fit of the scatter plot (black lines). In fact, consider-

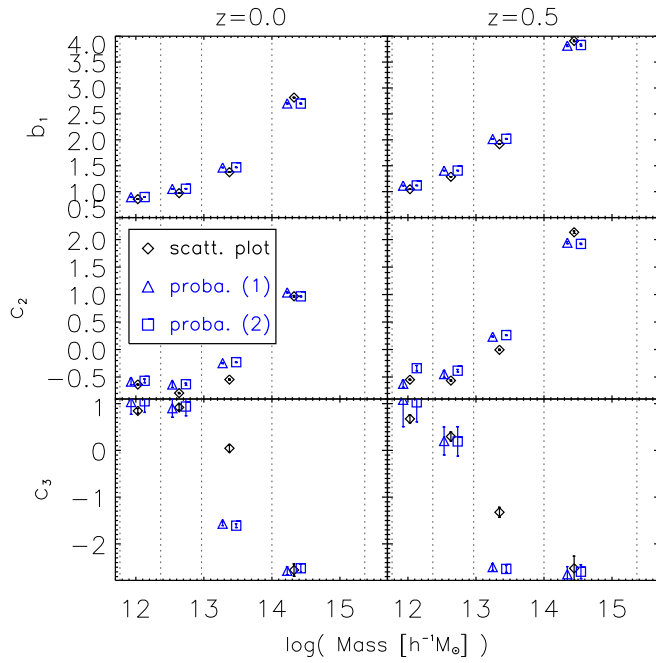


**Figure A4.** Bias coefficients obtained by fitting the scatter plot on scales between  $40$  and  $80h^{-1}\text{Mpc}$  with respect to the average mass of the haloes.

ing Fig. A4 which summarizes the measurements of the bias coefficients from the two presented methods one can remark that despite small discrepancies the overall behavior of the bias coefficients with respect to the mass is qualitatively in good agreement. Note that the obtained linear bias from the probability density function of fluctuation is in impressive agreement with linear bias obtained from the 2-point cross-correlation function (see Fig. 1).